Supplementary Material (ESI) for Chemical Communications
This journal is © The Royal Society of Chemistry 2007

Fluorescent dyes of esculetin and alizarin families respond to zinc ion ratiometrically

Lu Zhang, Shen Dong, and Lei Zhu*

Department of Chemistry and Biochemistry, Florida State University, Tallahassee, FL 32306

Electronic Supplementary Information

Determination of association constant (K_a) between $Zn(ClO_4)_2$ and ML

A solution of 4-methylesculetin (ML, 68 μM) and $Zn(ClO_4)_2$ (575 μM) was titrated incrementally into a semi-micro quartz cuvette (Starna®) containing a solution of ML (750 μL, 68 μM) at room temperature. The absorbance change (ΔA) was plotted against the total concentration of Zn^{2+} ($[Zn]_t$) at 394 nm (Fig. S1A). The association constant (K_a) was determined through least squares regression curve-fitting of the data at 394 nm with a 1:1 binding isotherm equation (Origin® 5.0) [1].

A solution of ML (6.8 μM) and $Zn(ClO_4)_2$ (575 μM) was titrated into a semi-micro quartz fluorescence cuvette (Starna®) containing a solution of ML (750 μL, 6.8 μM) at room temperature. The fluorescence intensity ratio (I_F/I_0) at 520 nm was plotted against $[Zn]_t$ (Fig. S1B). The association constant (K_a) was determined through least squares regression curve-fitting of the data at 520 nm with a 1:1 binding isotherm equation (Origin® 5.0) [2].

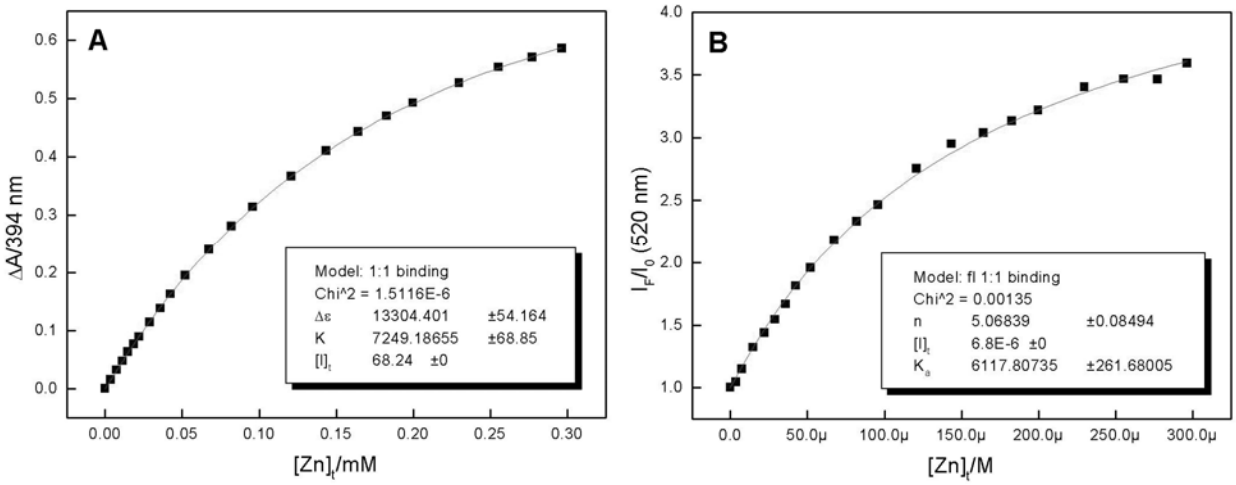

Figure S1. (A) Absorbance change ($\Delta A = A - A_0$) of ML (68 μM) at 394 nm in 75% methanol buffered with 10 mM HEPES at pH 7.1 in the presence of 0 – 297 μM of $Zn(ClO_4)_2$. The solid line is a theoretical 1:1 binding curve of ΔA *vs.* $[Zn]_t$. (B) Fluorescence intensity increase (I_F/I_0, λ_{ex} = 394 nm) of ML (6.8 μM) at 520 nm in the presence of 0 – 297 μM of $Zn(ClO_4)_2$. The solid line is a theoretic curve of fluorescence intensity ratio (I_F/I_0) *vs.* $[Zn]_t$ fitted with a 1:1 binding isotherm equation (Origin® 5.0).

Absorption (Fig. S2) and fluorescence (Fig S3) titrations of esculetin (EL) with $Zn(BF_4)_2$

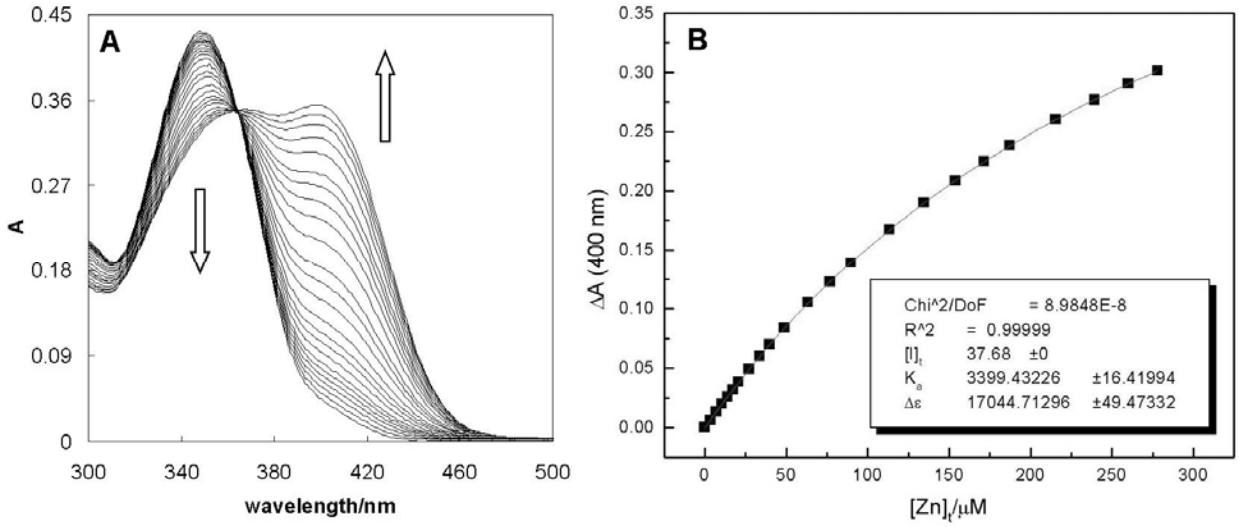

Figure S2. (A) The absorption spectra of esculetin (EL, 38 μM) in 75% methanol (10 mM HEPES at pH 7.0) in the presence of 0 – 293 μM of $Zn(BF_4)_2$. The arrows indicate spectral change with increasing $[Zn]_t$. (B) Absorbance change (ΔA) of EL (38 μM) at 400 nm with increasing $[Zn]_t$. The solid line is a theoretical 1:1 binding curve of ΔA *vs.* $[Zn]_t$.

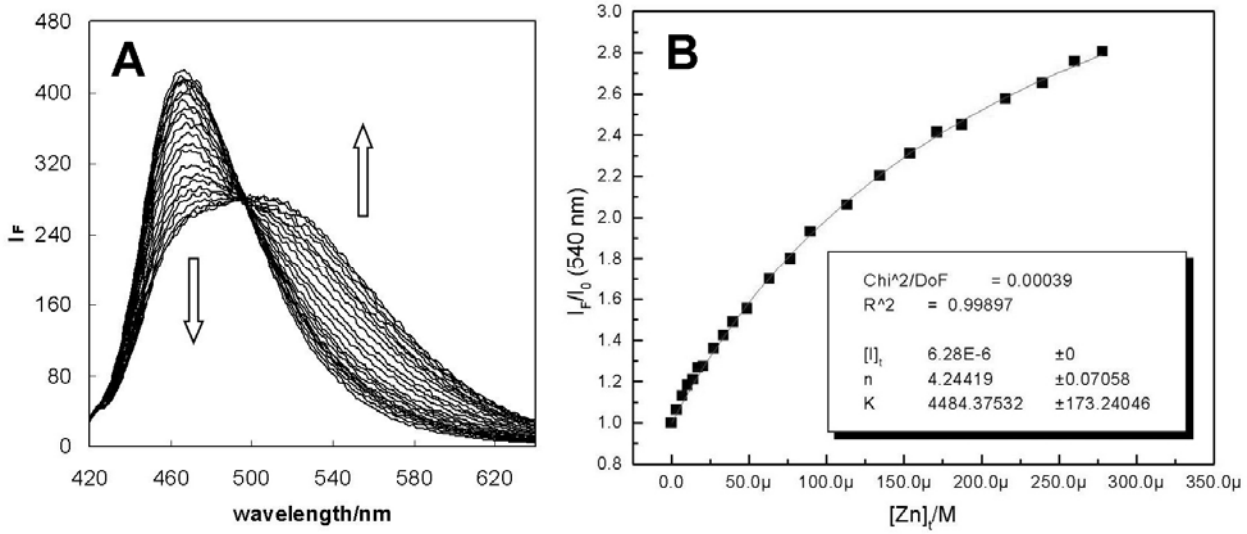

Figure S3. (A) The fluorescence spectra of EL (6.3 μM, λ_{ex} = 400 nm) in 75% methanol (10 mM HEPES at pH 7.0) in the presence of 0 – 293 μM of $Zn(BF_4)_2$. The arrows indicate spectral change with increasing $[Zn]_t$. (B) Fluorescence intensity increase (I_F/I_0, λ_{ex} = 400 nm) of EL (6.3 μM) at 540 nm with increasing $[Zn]_t$. The solid line is a theoretic curve of I_F/I_0 *vs.* $[Zn]_t$ at 540 nm fitted with a 1:1 binding isotherm equation (Origin® 5.0).

Spectrophotometric titrations of alizarin red S (ARS) with Zn^{2+}

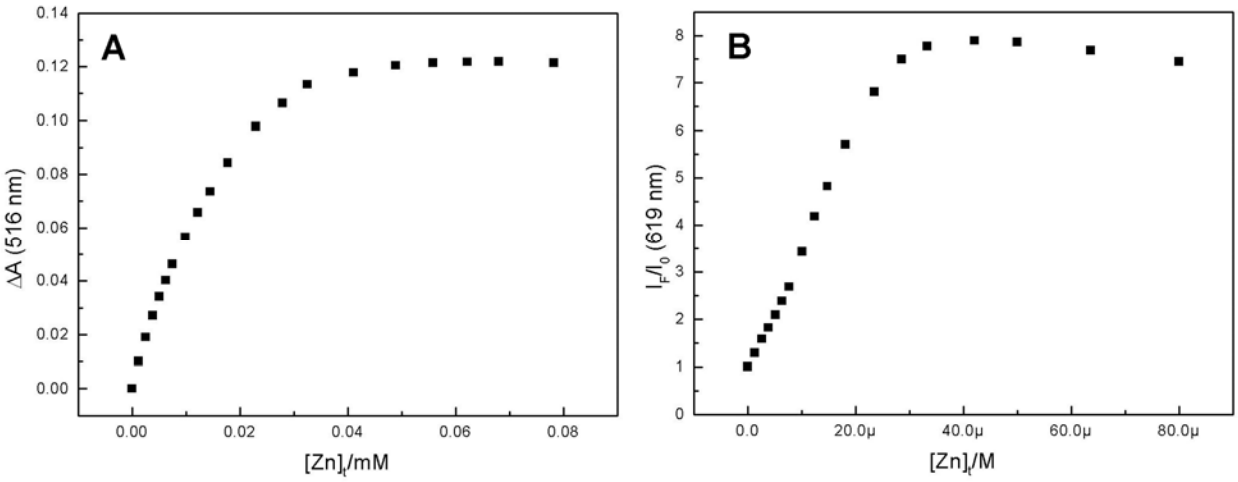

Figure S4. (A) Absorption and (B) fluorescence (λ_{ex} = 530 nm) responses of ARS (29 μM) to $[Zn]_t$ in 75% methanol (10 mM HEPES at pH 7.1).

Spectrophotometric titrations of alizarin (AZ) with $Zn(BF_4)_2$

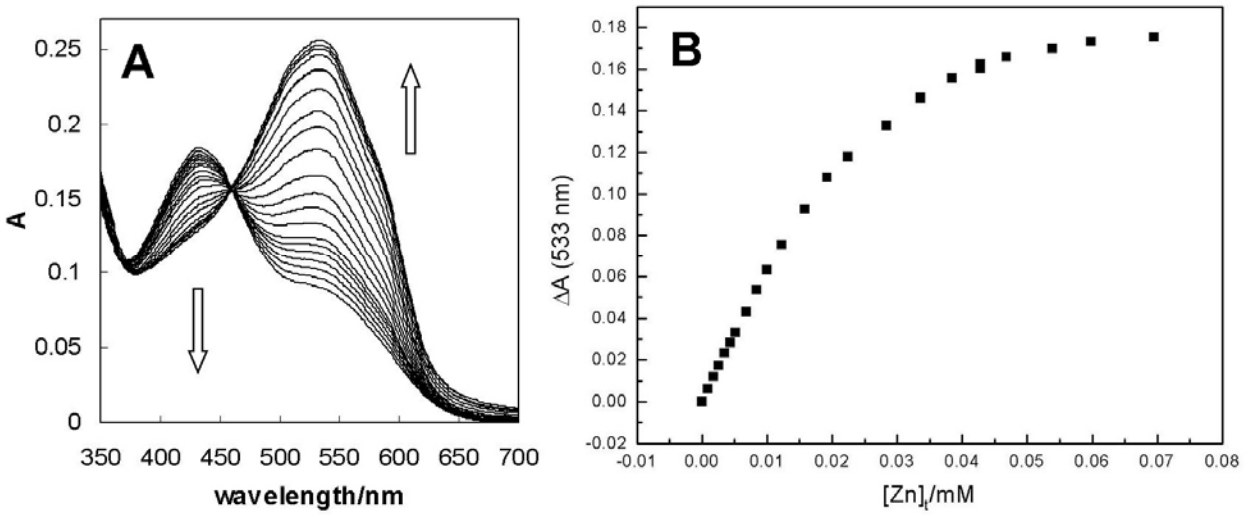

Figure S5. (A) The absorption spectra of alizarin (39 μM) in 75% methanol (25 mM HEPES at pH 7.0) in the presence of 0 – 69 μM of $Zn(BF_4)_2$. The arrows indicate spectral change with increasing $[Zn]_t$. (B) Absorbance change (ΔA) of alizarin (39 μM) at 533 nm with increasing $[Zn]_t$.

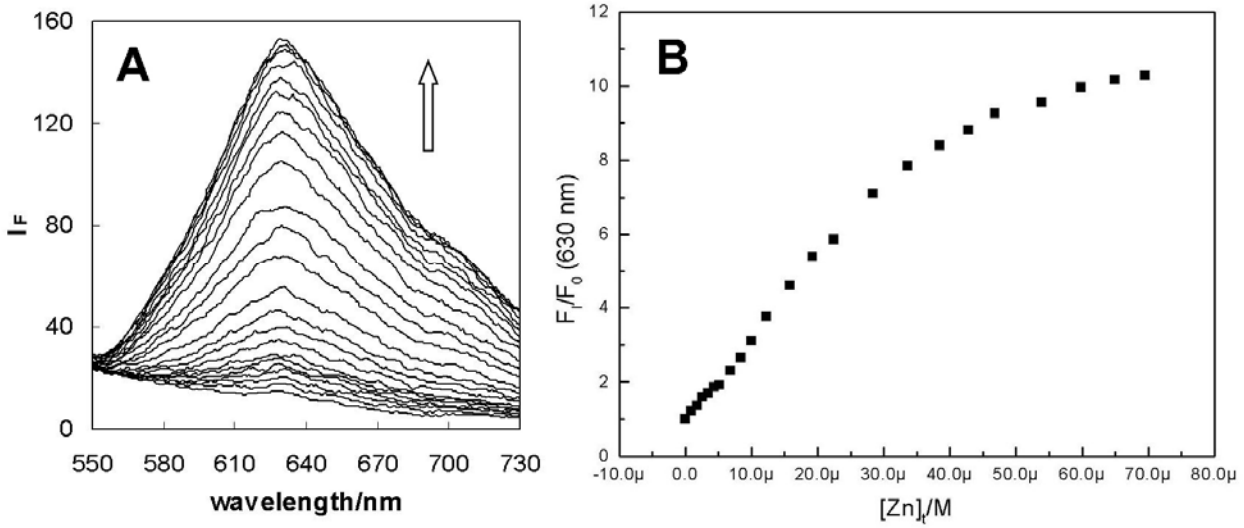

Figure S6. (A) The fluorescence spectra of alizarin (29 μM, λ_{ex} = 533 nm) in 75% methanol (25 mM HEPES at pH 7.0) in the presence of 0 – 69 μM of $Zn(BF_4)_2$. The arrow indicates spectral change with increasing $[Zn]_t$. (B) Fluorescence intensity increase (I_F/I_0, λ_{ex} = 533 nm) of alizarin (29 μM) at 630 nm with increasing $[Zn]_t$.

Procedure for Job plots

The total molar concentration of a dye and a metal ion is held constant, but their mole fractions are varied. The absorbance that is proportional to complex formation is plotted against the mole fractions of either component. The point of discontinuity is found by extrapolating the two approximately linear segments. The association stoichiometry is calculated from the ratio of mole fraction at the point of discontinuity [3, 4].

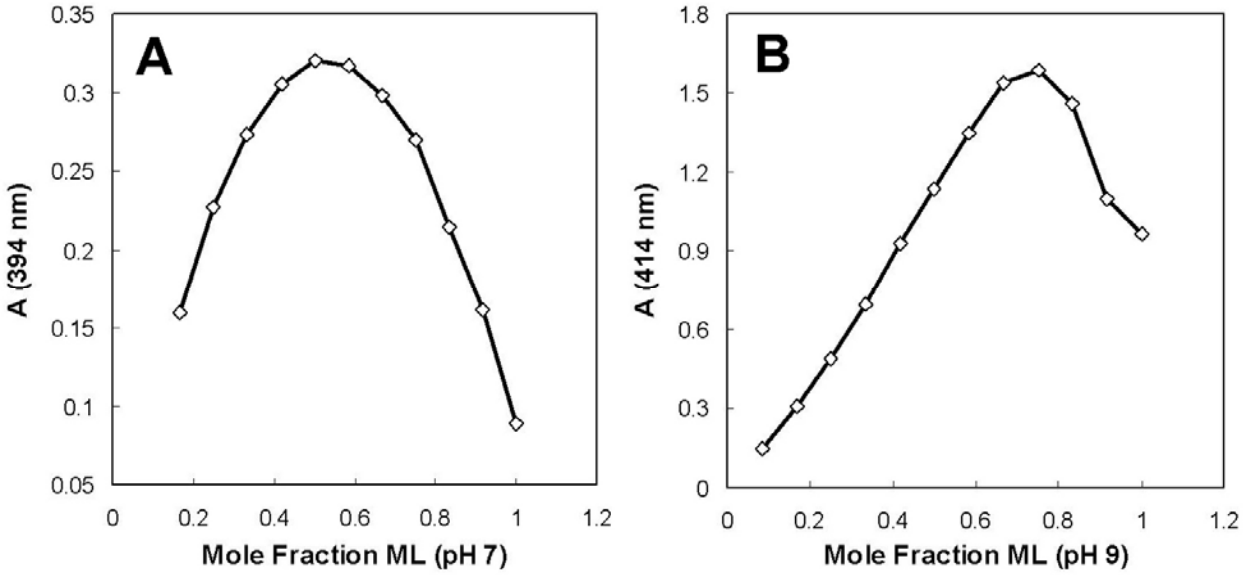

Figure S7. (A) Job plot for ML association with Zn^{2+} (75% MeOH, 10 mM HEPES, pH 7.0). The total molar concentration of ML and Zn^{2+} is 164 μM. The mole fraction of ML was continuously varied from 0 to 1. (B) Job plot for ML association with Zn^{2+} (75% MeOH, 25 mM CHES, pH 9.0). The total molar concentration was 205 μM.

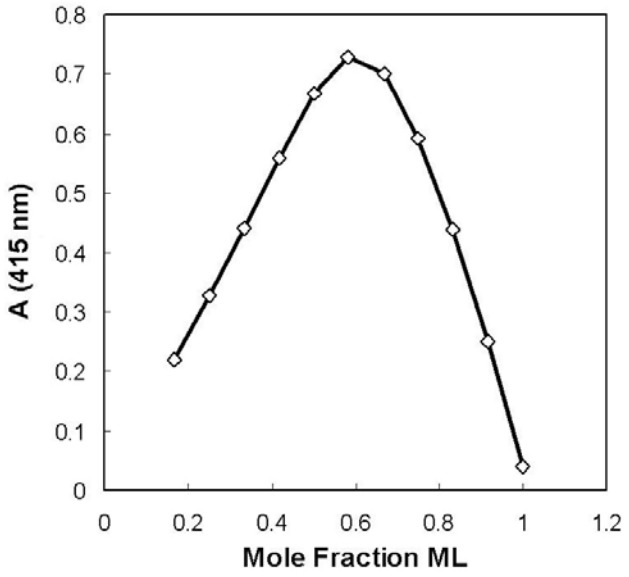

Figure S8. Job plot for ML association with Cu^{2+} (75% MeOH, 25 mM HEPES, pH 7.0). The total molar concentration of ML and Cu^{2+} is 153 μM. The mole fraction of ML was continuously varied from 0 to 1.

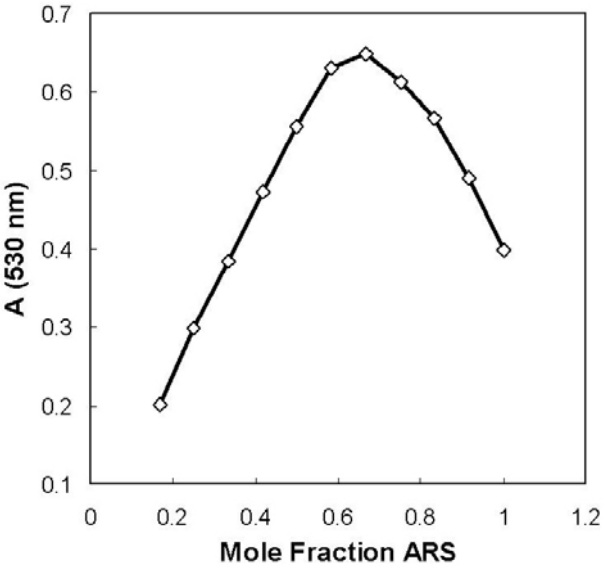

Figure S9. Job plot for ARS association with Zn^{2+} (75% MeOH, 25 mM HEPES, pH 7.0). The total molar concentration of ML and Zn^{2+} is 176 μM. The mole fraction of ML was continuously varied from 0 to 1.

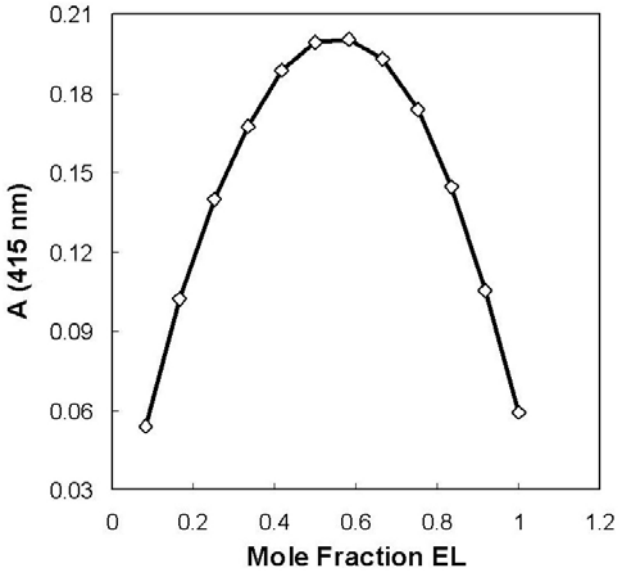

Figure S10. Job plot for EL association with Zn^{2+} (75% MeOH, 25 mM HEPES, pH 7.0). The total molar concentration of ML and Zn^{2+} is 151 μM. The mole fraction of ML was continuously varied from 0 to 1.

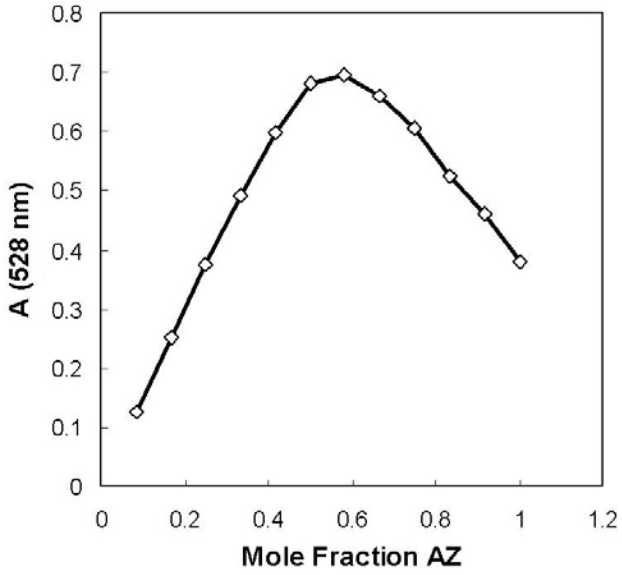

Figure S11. Job plot for AZ association with Zn^{2+} (75% MeOH, 25 mM HEPES, pH 7.0). The total molar concentration of ML and Zn^{2+} is 176 μM. The mole fraction of ML was continuously varied from 0 to 1.

Procedure for quantum yield determination [5, 6]

Fluorescence quantum yield were determined in 75% methanol with 10 mM HEPES buffer at pH 7.0 by using solutions of quinine sulfate (Φ_f = 0.546, 0.5 M H_2SO_4) and rhodamine 6G (Φ_f = 0.95, ethanol) as standards. The excitation wavelengths are the λ_{max} of the respective species. The quantum yields can be calculated using Equation 1:

$$\Phi_u = [(A_s F_u n^2) / (A_u F_s n_0^2)] \Phi_s \qquad (1)$$

Where A_s and A_u are the absorbance of the samples and reference solutions at their excitation wavelengths, F_s and F_u are the corresponding integrated fluorescence areas, and n is the refractive index of the solvent of the sample (n) or of the standard (n_0). Absorbance of samples and standards was kept below 0.1.

pH-dependent absorption and fluorescence studies

Stock buffer solutions (50 mM) of various pH values were prepared in 75% methanol. PHP (potassium hydrogen phthalate, pH 2.5 – 5.0), MES (2-morpholineoethanesulfonic acid, pH 5.5 – 6.5), HEPES (4-(2-hydroxyethyl)piperazine-1-ethanesulfonic acid, pH 7.0 – 8.0), EPPS (4-(2-hydroxyethyl)piperazine-1-propanesulfonic acid, pH 8.2 – 8.5), and CHES (2-(cyclohexylamino)-1-ethanesulfonic acid, 9.0 – 10.0) were used to cover different pH ranges. Final concentrations were the following: 4.0 μM of ML and 49.5 mM of buffer were used for both absorption and fluorescence measurements; 32 μM of ARS and 46 mM of buffer were used for both absorption and fluorescence measurements. The solvent was 75% methanol.

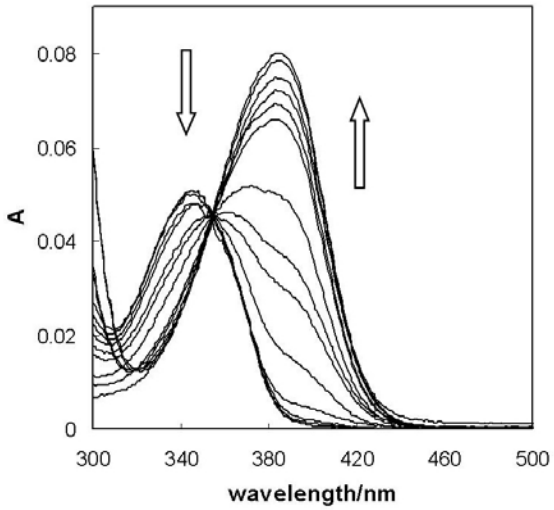

Figure S12. Absorption spectral change of ML (4.0 μM in 75% methanol with 49.5 mM buffer) with increasing pH value as indicated by the arrows.

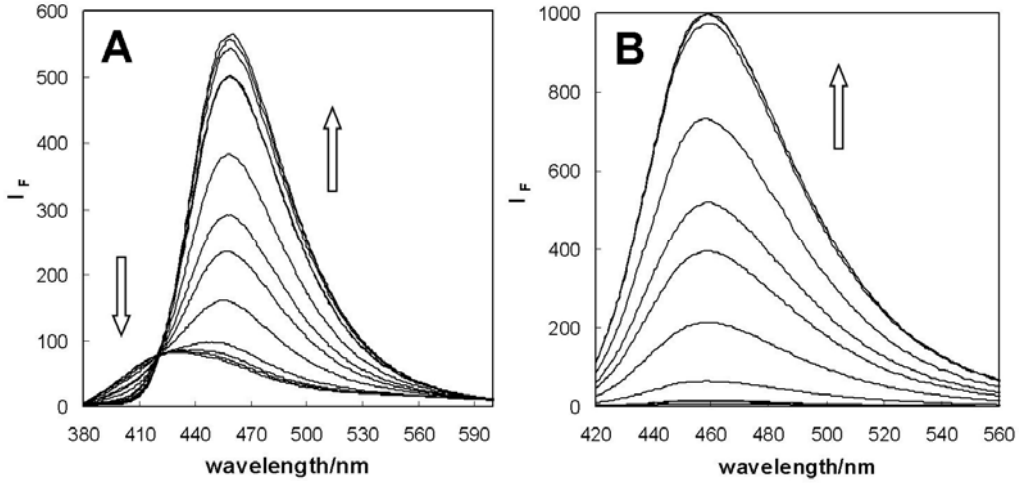

Figure S13. Fluorescence spectral change of ML (4.0 μM in 75% methanol with 49.5 mM buffer) with increasing pH value as indicated by the arrows. (A) λ_{ex} = 348 nm; (B) λ_{ex} = 394 nm.

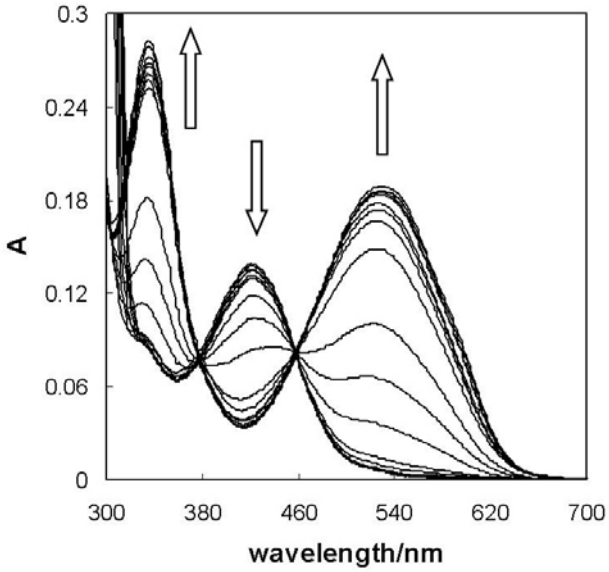

Figure S14. Absorption spectral change of ARS (32 μM in 75% methanol with 46 mM buffer) with increasing pH value as indicated by the arrows.

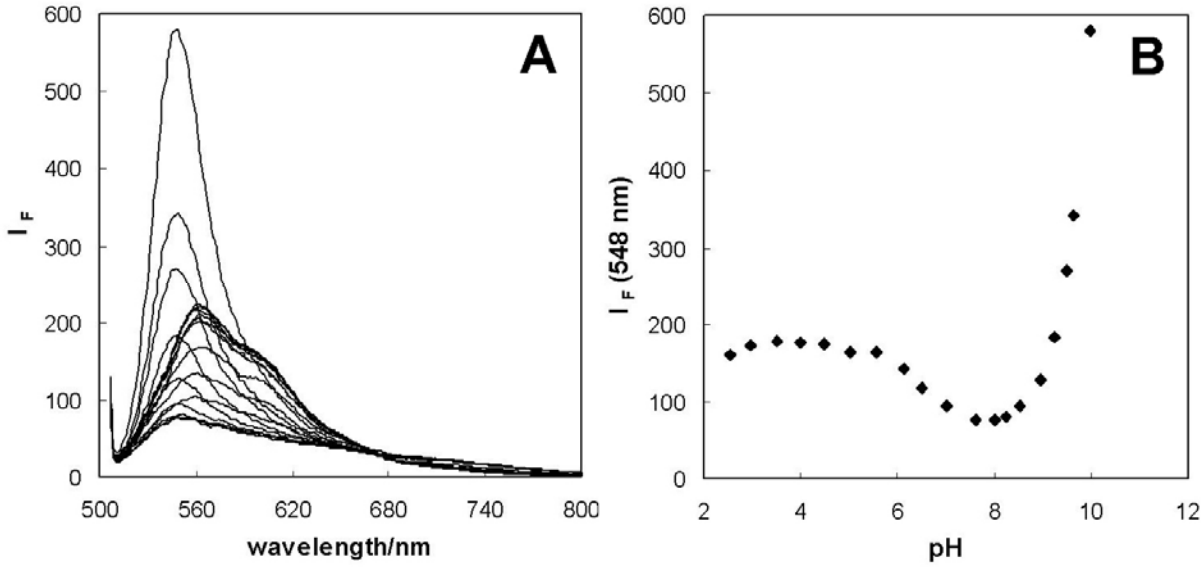

Figure S15. (A) Fluorescence spectra of ARS (32 μM in 75% methanol with 46 mM buffer) at various pH values. (B) Fluorescence intensity at 548 nm was plotted against pH values. Two transitions were revealed.

K_a dependence on pH

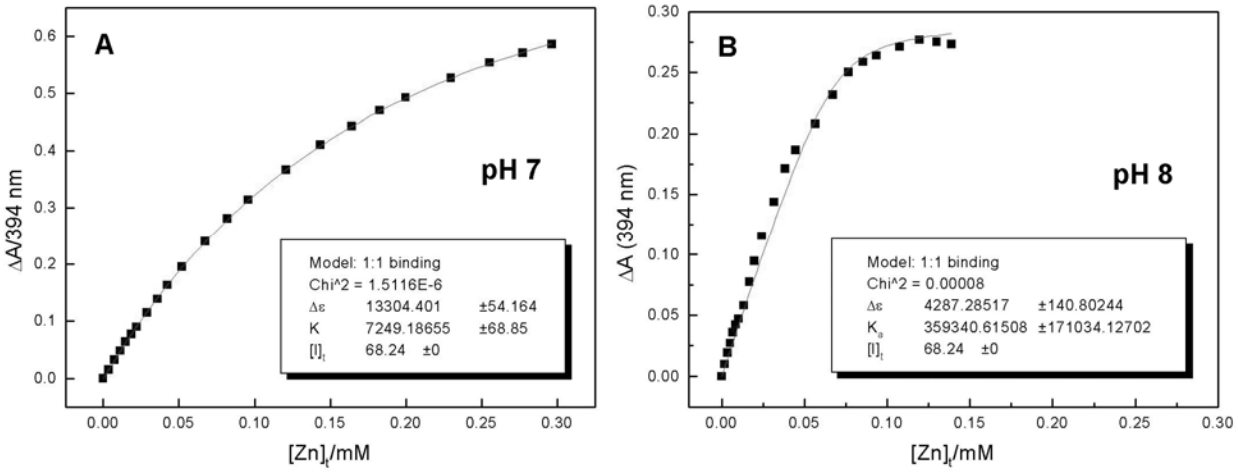

Figure S16. Absorbance change ($\Delta A = A - A_0$, squares) of ML (68 μM) at (A) pH 7 and (B) pH 8 with increasing $[Zn]_t$. The solid lines are theoretical 1:1 binding curves of ΔA *vs.* $[Zn]_t$. both x-axis's are scaled to 0.3 mM for comparison.

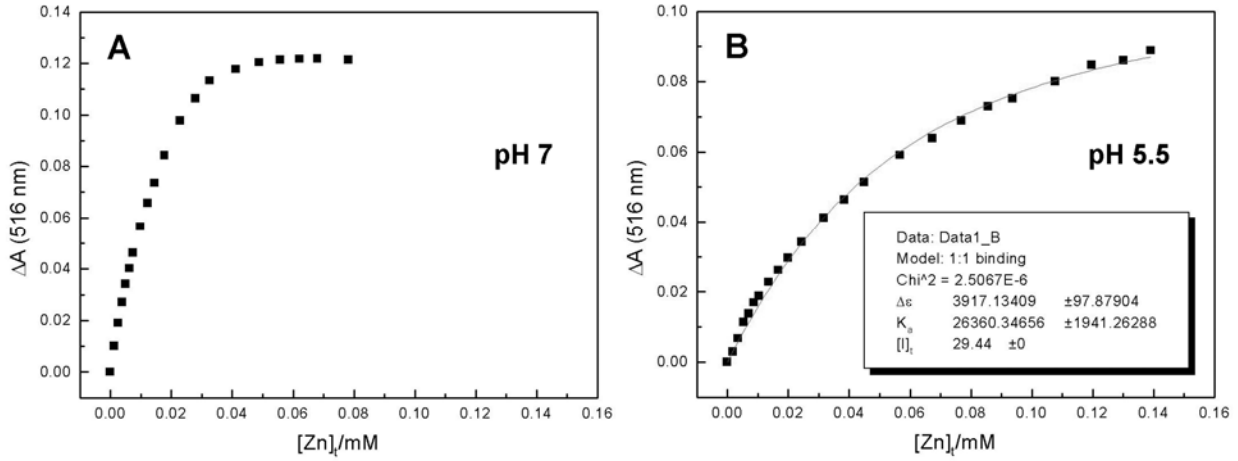

Figure S17. Absorbance changes ($\Delta A = A - A_0$, squares) of ARS (29 μM) at (A) pH 7 and (B) pH 5.5 with increasing $[Zn]_t$. The solid line in (B) is a theoretical 1:1 binding curve of ΔA *vs.* $[Zn]_t$. Both x-axis's are scaled to 0.16 mM for comparison.

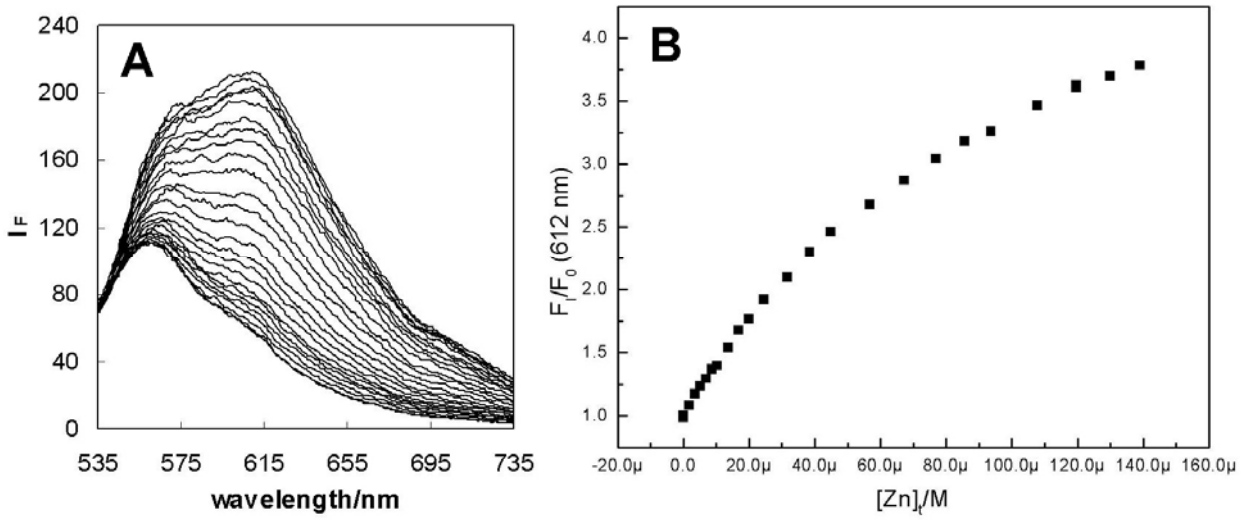

Figure S18. (A) The fluorescence spectra of ARS (29 μM, λ_{ex} = 530 nm) in 75% methanol (25 mM MES at pH 5.5) in the presence of 0 – 139 μM of $Zn(BF_4)_2$. (B) Fluorescence intensity increase (I_F/I_0, λ_{ex} = 394 nm) of ARS (squares, 29 μM) with increasing $[Zn]_t$. The absorbance of the sample was too large (> 0.1) for fluorescence intensity to have linear response to concentration. Therefore, curve fitting was not used.

Metal ion selectivity of ML (Ca^{2+}, Cd^{2+}, Mg^{2+}, Fe^{2+}, Pb^{2+}, and Cu^{2+})

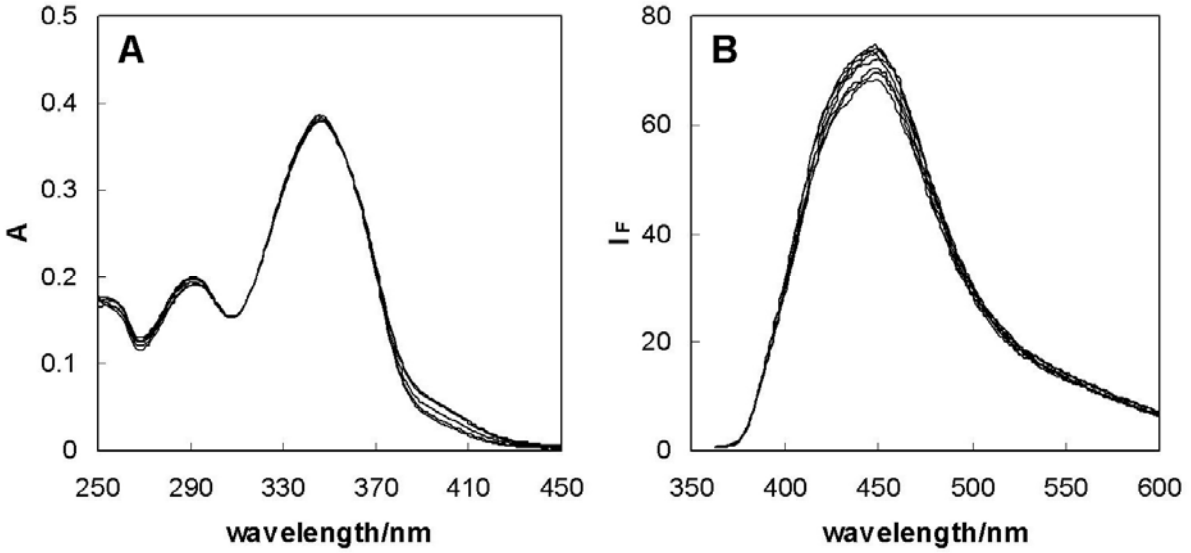

Figure S19. (A) The absorption spectra of ML (32 μM) in 75% methanol (10 mM HEPES at pH 7.0) in the presence of 0 – 241 μM of $Ca(ClO_4)_2$. (B) The fluorescence spectra of ML (3.2 μM, λ_{ex} = 394 nm) in 75% methanol (10 mM HEPES at pH 7.1) in the presence of 0 – 27 μM of $Ca(ClO_4)_2$.

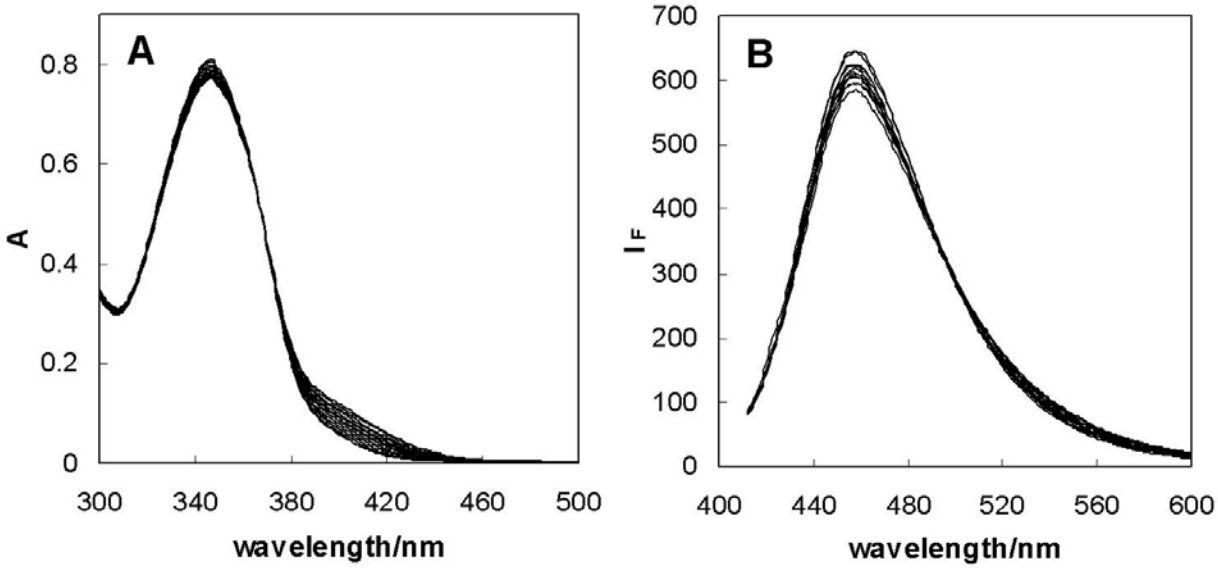

Figure S20. (A) The absorption spectra of ML (68 μM) in 75% methanol (10 mM HEPES at pH 7.1) in the presence of 0 – 258 μM of $Cd(ClO_4)_2$. (B) The fluorescence spectra of ML (6.8 μM, λ_{ex} = 394 nm) in 75% methanol (10 mM HEPES at pH 7.1) in the presence of 0 – 258 μM of $Cd(ClO_4)_2$.

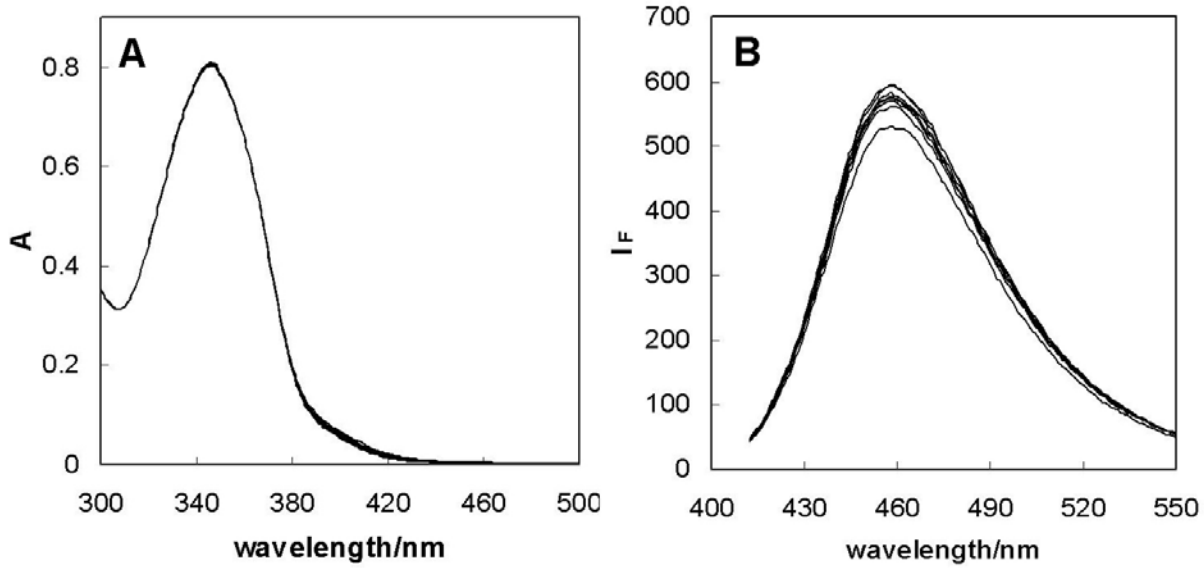

Figure S21. (A) The absorption spectra of ML (68 μM) in 75% methanol (10 mM HEPES at pH 7.1) in the presence of 0 – 258 μM of $Mg(ClO_4)_2$. (B) The fluorescence spectra of ML (6.8 μM, λ_{ex} = 394 nm) in 75% methanol (10 mM HEPES at pH 7.1) in the presence of 0 – 258 μM of $Mg(ClO_4)_2$.

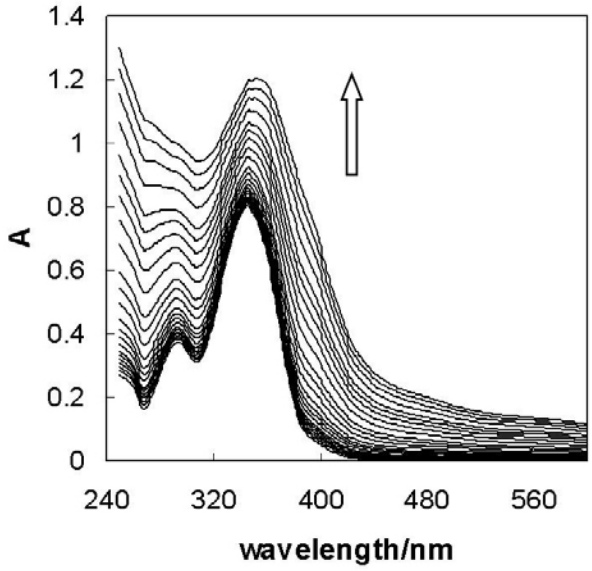

Figure S22. (A) The absorption spectra of ML (68 μM) in 75% methanol (10 mM HEPES at pH 7.1) in the presence of 0 – 258 μM of $Fe(ClO_4)_2$. The increase of absorbance across the spectrum upon addition of Fe(II) is due to the absorption from increasing $[Fe^{2+}]$.

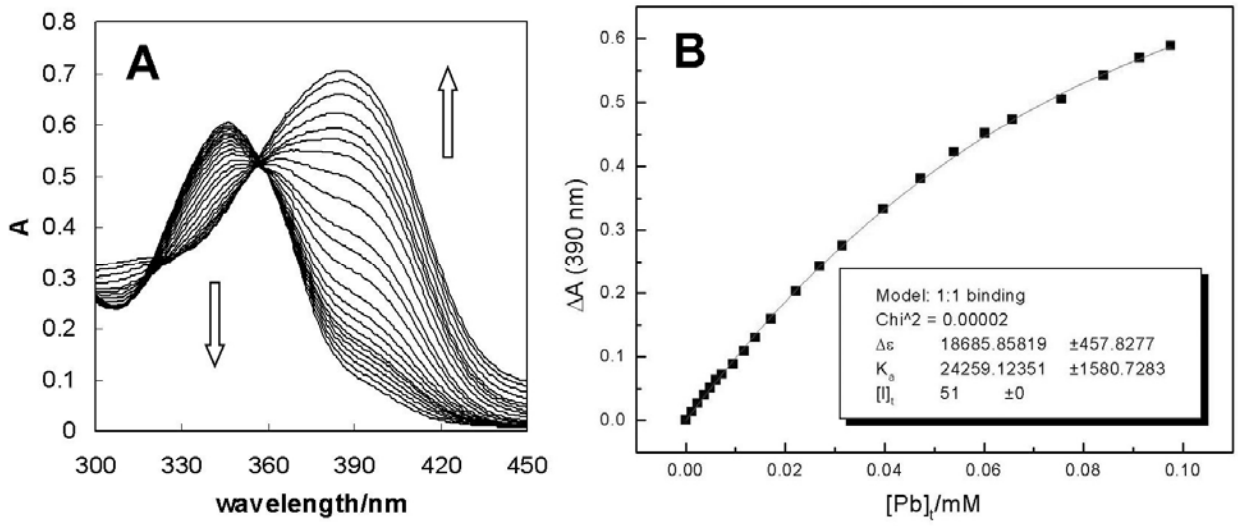

Figure S23. (A) The absorption spectra of ML (51 μM) in 60% methanol (25 mM HEPES at pH 7.0) in the presence of 0 – 97 μM of $Pb(NO_3)_2$. The arrows indicate spectral change with increasing $[Pb]_t$. (B) Absorbance change ($\Delta A = A - A_0$) of ML (51 μM) at 390 nm with increasing $[Pb]_t$. The solid line is a theoretical 1:1 binding curve of ΔA *vs.* $[Pb]_t$.

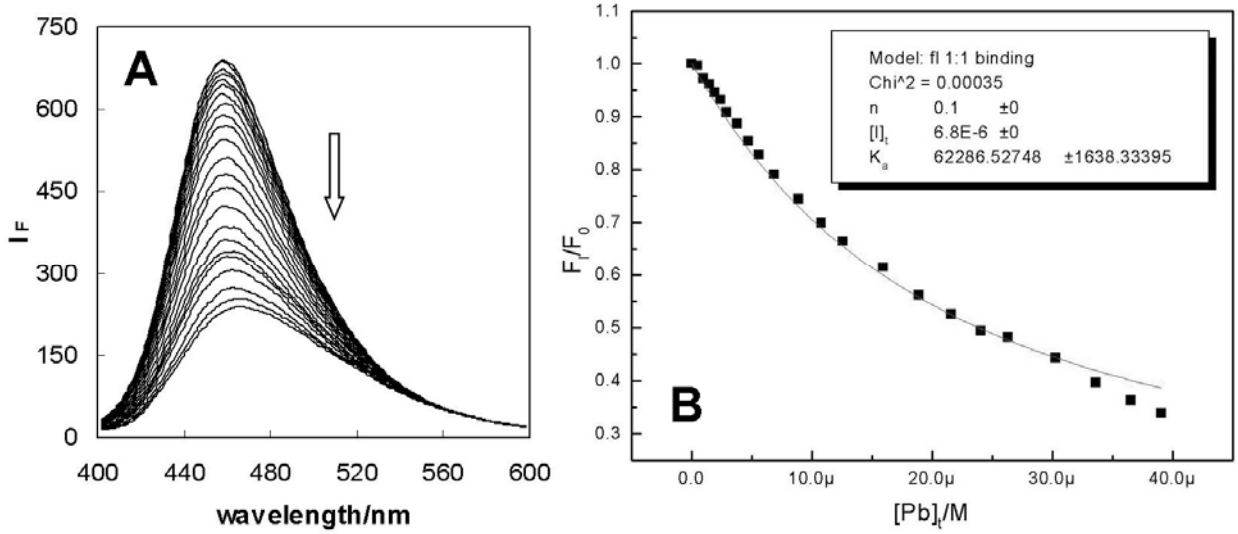

Figure S24. (A) The fluorescence spectra of ML (6.8 μM, λ_{ex} = 394 nm) in 60% methanol (25 mM HEPES at pH 7.0) in the presence of 0 – 39 μM of $Pb(NO_3)_2$. (B) Fluorescence intensity decrease (I_F/I_0, λ_{ex} = 394 nm) of ML (6.8 μM) with increasing $[Pb]_t$. The solid line is a theoretic curve of I_F/I_0 *vs.* $[Pb]_t$ fitted with a 1:1 binding isotherm equation (Origin® 5.0).

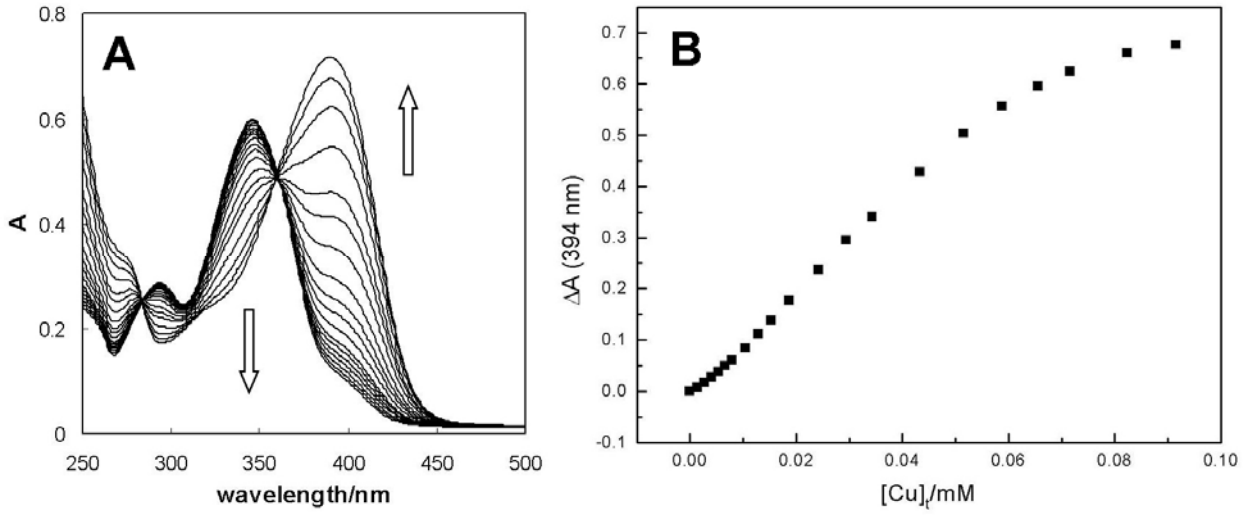

Figure S25. (A) The absorption spectra of ML (51 μM) in 60% methanol (25 mM HEPES at pH 7.0) in the presence of 0 – 92 μM of $Cu(NO_3)_2$. The arrows indicate spectral change with increasing $[Cu]_t$. (B) Absorbance change ($\Delta A = A - A_0$) of ML (51 μM) at 394 nm with increasing $[Cu]_t$. The sigmoidal shape of the curve suggests higher order complexation than 1:1.

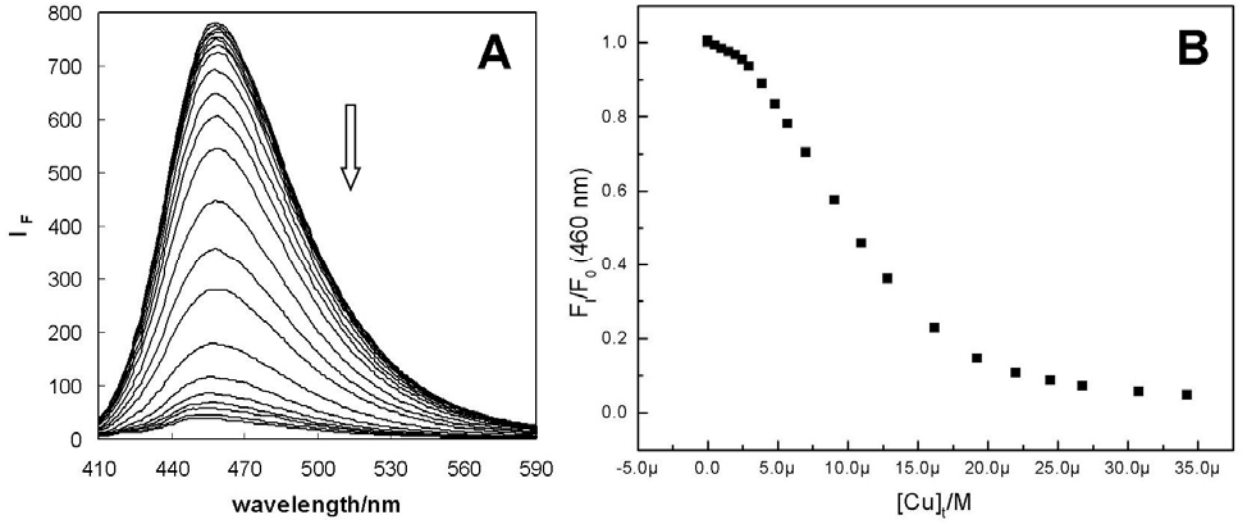

Figure S26. (A) The fluorescence spectra of ML (6.8 μM, λ_{ex} = 394 nm) in 60% methanol (25 mM HEPES at pH 7.0) in the presence of 0 – 34 μM of $Cu(NO_3)_2$. (B) Fluorescence intensity decrease (I_F/I_0, λ_{ex} = 394 nm) of ML (6.8 μM) with increasing $[Cu]_t$. The sigmoidal shape of the curve suggests higher order complexation than 1:1.

Metal ion selectivity of ARS (Ca^{2+}, Cd^{2+}, Mg^{2+}, and Pb^{2+})

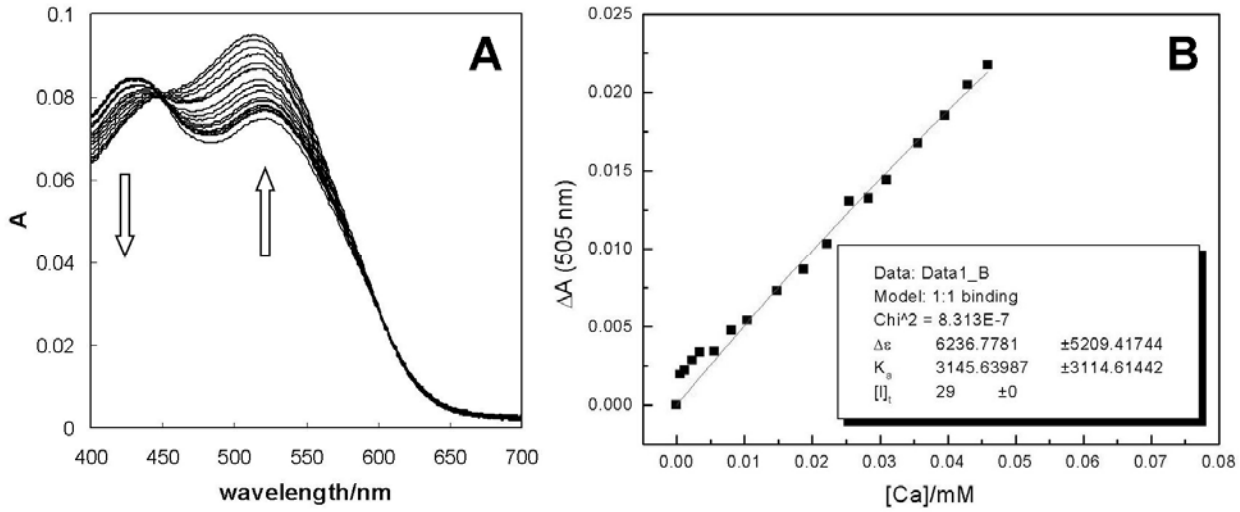

Figure S27. (A) The absorption spectra of ARS (29 μM) in 60% methanol (25 mM HEPES at pH 7.0) in the presence of 0 – 46 μM of $Ca(ClO_4)_2$. The arrows indicate spectral change with increasing $[Ca]_t$. (B) Absorbance change ($\Delta A = A - A_0$) of ARS (29 μM) at 505 nm with increasing $[Ca]_t$. The solid line is a theoretical 1:1 binding curve of ΔA *vs.* $[Ca]_t$.

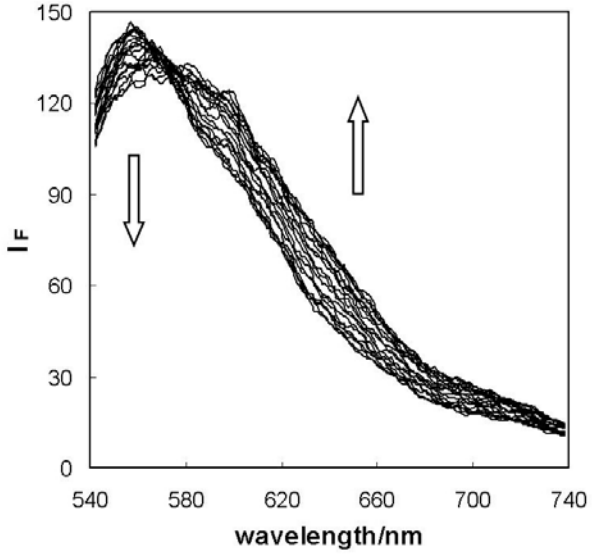

Figure S28. The fluorescence spectra of ARS (29 μM, λ_{ex} = 510 nm) in 60% methanol (25 mM HEPES at pH 7.0) in the presence of 0 – 46 μM of $Ca(ClO_4)_2$. The arrows indicate spectral change with increasing $[Ca]_t$.

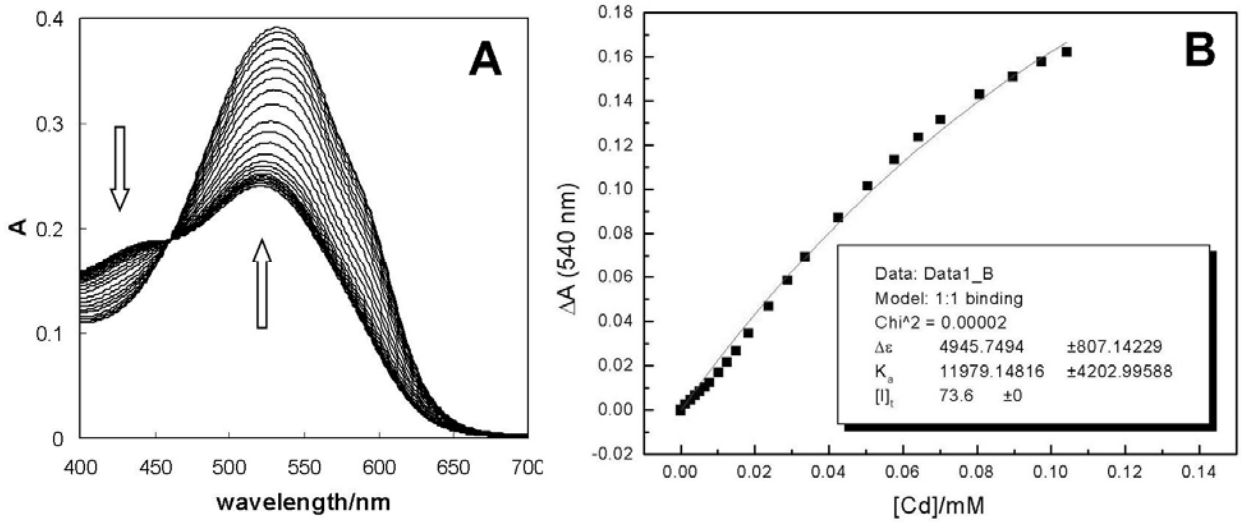

Figure S29. (A) The absorption spectra of ARS (74 μM) in 60% methanol (25 mM HEPES at pH 7.0) in the presence of 0 – 104 μM of $Cd(ClO_4)_2$. The arrows indicate spectral change with increasing $[Cd]_t$. (B) Absorbance change ($\Delta A = A - A_0$) of ARS (74 μM) at 540 nm with increasing $[Cd]_t$. The solid line is a theoretical 1:1 binding curve of ΔA *vs.* $[Cd]_t$.

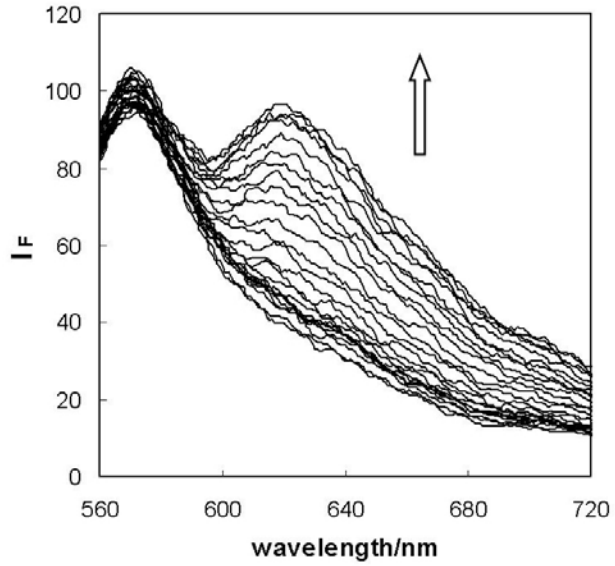

Figure S30. The fluorescence spectra of ARS (29 μM, λ_{ex} = 540 nm) in 60% methanol (25 mM HEPES at pH 7.0) in the presence of 0 – 52 μM of $Cd(ClO_4)_2$. The arrow indicates spectral change with increasing $[Cd]_t$.

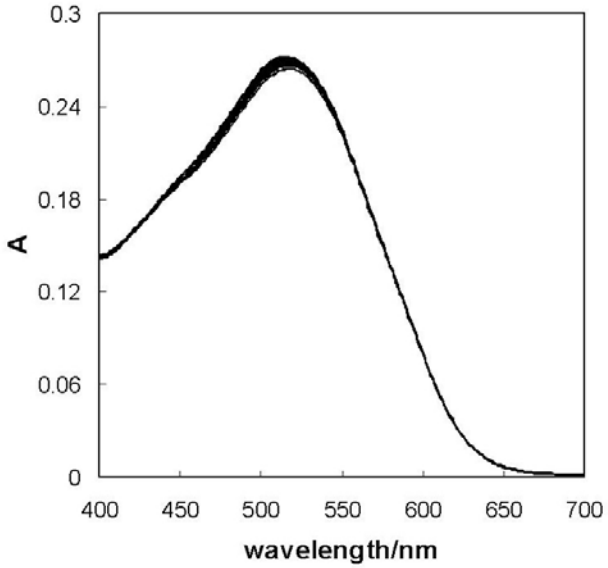

Figure S31. (A) The absorption spectra of ARS (74 μM) in 60% methanol (25 mM HEPES at pH 7.0) in the presence of 0 – 90 μM of $Mg(ClO_4)_2$.

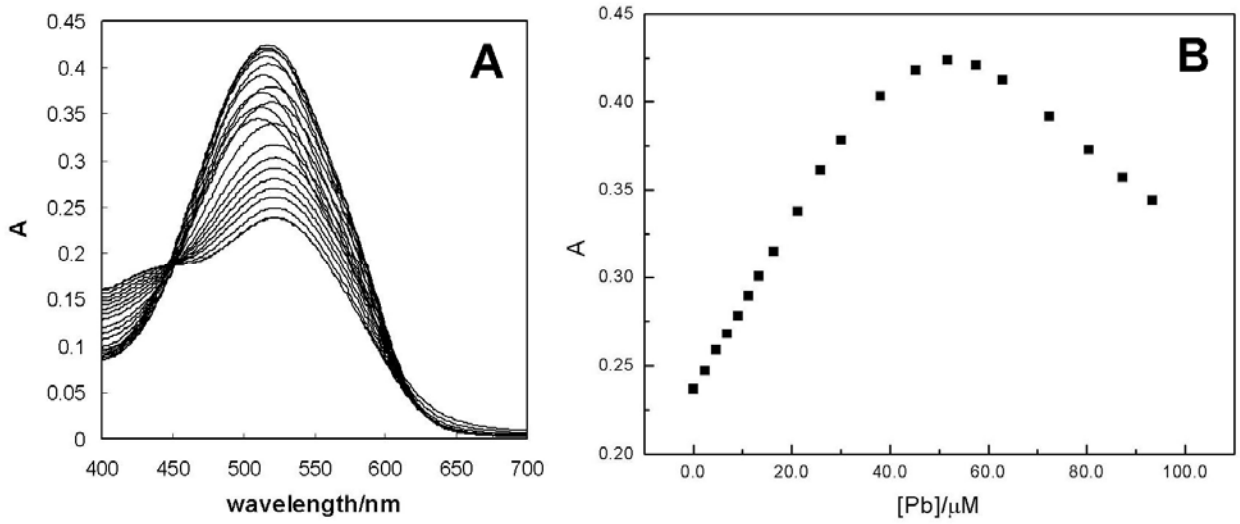

Figure S32. (A) The absorption spectra of ARS (74 μM) in 60% methanol (25 mM HEPES at pH 7.0) in the presence of 0 – 93 μM of $Pb(NO_3)_2$. (B) Absorbance at 515 nm was plotted against $[Pb]_t$.

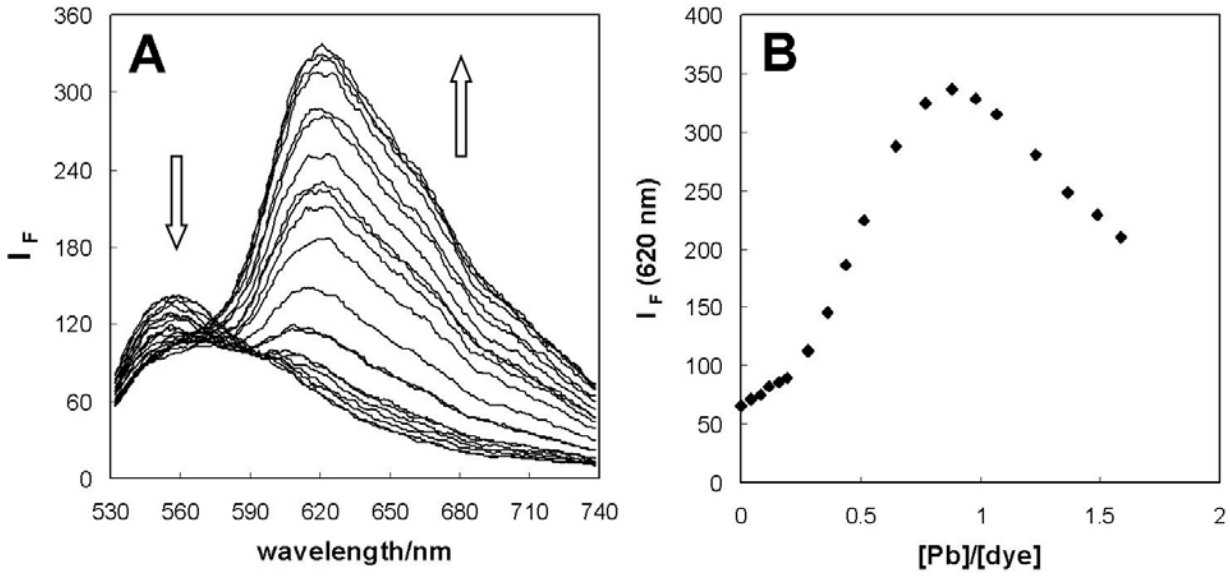

Figure S33. (A) The emission spectra of ARS (29 μM, λ_{ex} = 515 nm) in 60% methanol (25 mM HEPES at pH 7.0) in the presence of 0 – 47 μM of $Pb(NO_3)_2$. (B) Fluorescence intensity at 620 nm was plotted against $[Pb]_t$.

Computational Methods

The geometry of the structures was optimized using MM+ and ZINDO/1 methods in HyperChem 6.0, using Polak-Ribiere as the minimization algorithm. ZINDO/1 is a modified INDO version used for molecular systems containing transition metals. ZINDO/1 is a suitable semi-empirical method in HyperChem 6.0 for determining structures and energies of molecules containing transition metals in the first or second rows. HOMO and LUMO energies were also calculated on the basis of ZINDO/1 model and compiled in Table S1. Solvation was not taken into account in the calculation. Molecular orbitals were visualized using HyperChem 6.0.

	4-Methyleculetin		Esculetin	
	Free dye	Complex (Zn)	Free dye	Complex (Zn)
HOMO/ev	-6.740905	-6.694578	-6.851058	-7.072373
LUMO/ev	5.065339	4.001609	4.954028	3.931528
ΔE/ev	11.806244	10.696187	11.805086	11.003901

Table S1.

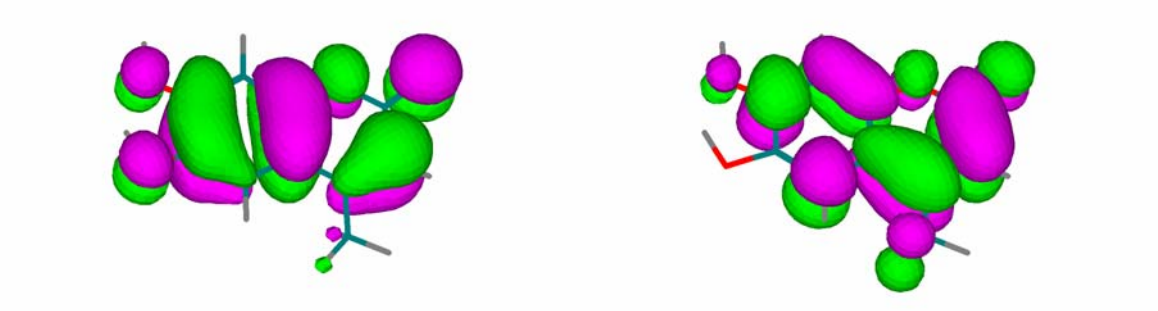

Figure S34. π (HOMO, left) and π* (LUMO, right) orbitals of 4-methylesculetin.

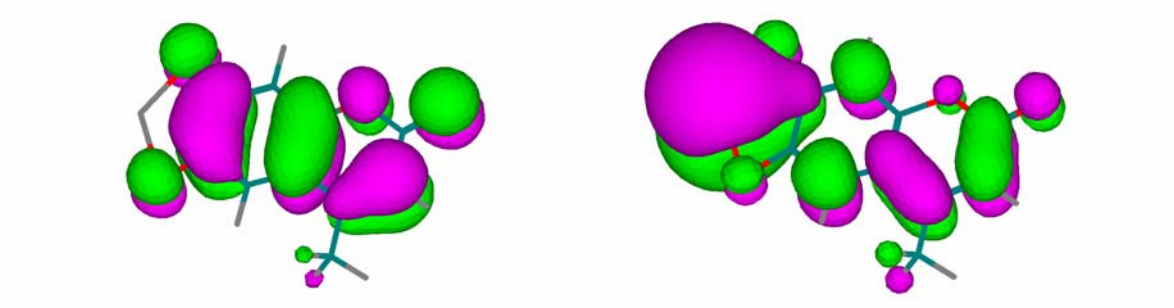

Figure S35. π (HOMO, left) and π* (LUMO, right) orbitals of 4-methylesculetin complex with Zn(II).

References Cited:

1. Zhu, L. and Anslyn, E.V., *Facile Quantification of Enantiomeric Excess and Concentration with Indicator-Displacement Assays: An Example in the Analyses of α-Hydroxyacids.* J. Am. Chem. Soc., 2004. **126**: p. 3676-3677.
2. Zhu, L., Zhong, Z., and Anslyn, E.V., *Guidelines in Implementing Enantioselective Indicator-Displacement Assays for a-Hydroxycarboxylates and Diols.* J. Am. Chem. Soc., 2005. **127**: p. 4260-4269.
3. Connors, K.A., *Binding Constants, The Measurement of Molecular Complex Stability.* 1987, New York: John Wiley and Sons.
4. Huang, C.Y., *Determination of Binding Stoichiometry by the Continuous Variation Method: The Job Plot.* Methods Enzymol., 1982. **87**: p. 509-525.
5. Fery-Forgues, S. and Lavabre, D., *Are Fluorescence Quantum Yields so Tricky to Measure? A Demonstration Using Familiar Stationary Products.* J. Chem. Ed., 1999. **76**: p. 1260-1264.
6. Du, H., Fuh, R.-C.A., Li, J., Corkan, L.A., and Lindsey, J.S., *PhotochemCAD††: A Computer-Aided Design and Research Tool in Photochemistry.* Photochem. Photobiol., 1998. **68**: p. 141-142.